Journal of Applied Mechanics and Technical Physics, Vol. 35, No. 3, 1994

EFFECT OF LONGITUDINAL ABERRATION IN AN ION-OPTICAL SYSTEM ON THE PROPERTIES OF A FOCUSED BEAM

V. N. Getmanov, I. M. Ikryanov, and O. Ya. Savchenko

UDC 621.384.65

Modelling of the processes involved in the passage of a beam through a system of high-voltage electrodes with allowance made for the thermal and grid spreads of transverse particle velocities constitutes a three-dimensional problem that is difficult to solve with modern computers. In the present work, an analytic method has been developed that reduces this problem to a two-dimensional one. The method corresponds to approximating a marked longitudinal aberration in an ion-optical system (IOS), when the effective emittance of the beam during its high-voltage shaping increases severalfold, this being characteristic of all IOS know thus far. Fully justified in this case is the statement that a unique relationship exists between the coordinates r and z, which respectively characterize the location of the particle on the emitter and the point of intersection of the axis by the particle (or the point of maximum approach of the particle to the axis), and also between r and α (α being the angle between the particle trajectory in the focusing region and the axis of the system). This statement leads to a hyperbolic law, established experimentally [1-3], of increase in current density in the central portion of the focused beam and thus confirms the validity of this law. When the motion of the particles in the near-axis portion of the focused beam is considered, additional use is made of the law of conservation of momentum in axisymmetric fields with respect to the axis; this stops the hyperbolic increase of current density and generates a practically constant level of the latter in this portion of the beam. The width of the near-axis portion of the beam and its convergence angle, both recorded by measuring the shape of the beam profile [4, 5], characterize the magnitude of the beam emittance supplied to the input of the IOS [3]. The beam emittance also affects the profile shape of the central portion of the beam, which deviates more from the hyperbolic shape, the higher the beam temperature. The relations between r and z and r and α necessary for calculating this shape were obtained by solving numerically the problems of [6]. The present paper gives the fundamental formulas characterizing the method and calculates the beam diameter in the crossover, the distribution of current density on the axis, and the profile shape of a focused proton beam allowing for the influence of the thermal spread of transverse velocities and of scattering by the grids. The calculations were compared with experimental data on the focusing of a 0.4-MeV proton beam with a current of 20-75 mA and a diameter of 2-5 mm in the crossover under conditions in which the effective emittance of the beam, as a result of aberrations during its high-voltage shaping, increased by a factor of 3 or more [1-3]. The shape of the accelerator electrodes, the distribution of potentials (in kilovolts), and the calculated trajectories for 20 current tubes at a total beam current of 61 mA and a beam diameter of 40 mm at the emitter are shown in Fig. 1, where the markers D8 and D9 denote the positions of multiwire beam profile sensors [2].

1. Calculation of Current Density in the Focused Beam Allowing for Longitudinal Aberration in the System of Beam-Shaping Electrodes. Figure 2 shows a diagram of the focusing of the particle beam by an axisymmetric electrostatic field onto segment ff_0. The current through a ring of width dx and radius x at a distance z from the plane of the entrance aperture is

$$dI = j(x, z)2\pi x dx = \sum^{k} j(r_k, 0)2\pi r_k \left| \frac{dr_k}{dz_k} \frac{dz_k}{dx} \right| dx, \tag{1.1}$$

where j(x, z) is the current density; k is the current tube number; z_k is the distance at which the particles traversing the ring intersect the axis; $j(r_k, 0)$ and r_k are the current densities of these particles and their distances from the axis in the plane of the entrance aperture. It follows from Eq. (1.1) that

Novosibirsk. Translated from Prikladnaya Mekhanika i Tekhnicheskaya Fizika, No. 3, pp. 3-13, May-June, 1994. Original article submitted June 21, 1993.

0021-8944/94/3503-0325$12.50

$$j(x, z) = \frac{1}{x}\sum^{k} j(r_k, 0) r_k \left|\frac{dr_k}{dz_k}\frac{dz_k}{dx}\right|.$$

Therefore, in the focusing region, as the axis is approached, the current density increases hyperbolically:

$$j(x, z) \to K(z)/x, \quad r_1 \to r_2 \to r, \quad K(z) = j(r, 0) \cot\alpha \frac{dr^2}{dz},$$

since α and r are dependent only on z.

As was shown by calculations [2] using the method of [6], over a wide range of regular divergence of the beam particles $\sqrt{m\nu_r^2/2}/r$ in the plane of the emitter, the dependences of z and r cot α on r are nearly linear:

$$z = f_0 - (f_0 - f)r/R, \quad r\cot\alpha = b + cr, \quad c < 0 \tag{1.2}$$

(Fig. 3a, b). The terms in Eq. (1.2) give a linear approximation in the description of longitudinal aberration. Using the values of parameters f_0, f, b, c, obtained as a result of mathematical modelling, one can calculate the distribution of current density over the entire range of x values, assuming that the bending of the particle trajectory in the beam-focusing region is neglected. According to Fig. 4, allowing for Eqs. (1.2) we have

$$z_1 = z + x\cot\alpha_1 = z + cx + b(f_0 - f)x/R(f_0 - z_1),$$
$$z_2 = z - x\cot\alpha_2 = z - cx - b(f_0 - f)x/R(f_0 - z_2),$$

whence

$$z_1^{\pm} = f_0 - f_-(1 \pm s_-)/2, \quad z_2^{\pm} = f_0 - f_+(1 \pm s_+)/2, \tag{1.3}$$

where

$$f_\pm = f_0 - z \pm cx; \quad s_\pm = \sqrt{1 \pm \beta_\pm};$$
$$\beta_\pm = 4b(f_0 - f)x/Rf_\pm^2.$$

Equations (1.3) in four variants give the relationship between the point of intersection of the axis by the current tube $z_1^{\pm}$ and $z_2^{\pm}$ and the observation point of the current in the focused beam z, x. At a fixed z, the set of all possible values $z_{1,2}^{\pm}$ satisfying the condition

$$f \leqslant z_{1,2}^{\pm} \leqslant f_0, \tag{1.4}$$

delimit the region of possible x values. The result of such analysis of Eqs. (1.3) in reflected in Fig. 5, which shows five different variants of the regions of the relationship between x and z. Figure 5 gives a clear representation of the nature of the distribution of current density in the focused beam. In region 1, all of which corresponds to $z < f$, where intersection of the z axis with the particles is impossible, the current is produced by current tubes corresponding only to the root z_1^-, since $x \to 0$ as $z_1^- \to f_0$ and $z_1^+ \to z < f$, which contradicts (1.4). The straight line separating regions 1 and 2 arises from the condition $z_1^+ = f$ (since $\partial z_1^+/\partial z > 0$ and $\partial z_1^+/\partial x > 0$) and corresponds to the steepest crossing of the z axis (at angle α_0 = arctan (c + b/R)) by particles which have escaped from the edge of the emitter, where r = R. When r < R, the particles corresponding to this variant of the solution z_1^+ cross the z axis when z > f at angles smaller than α_0, and produce a current through an area of radius x in regions 1-3. Similarly from the condition $z_2^+ = f$, a straight line separating regions 2 and 3 is obtained that bounds regions 4 and 5 from above. The curved line bounding regions 2 and 3 from above is obtained from the condition of existence of a root common to z_1^+ and z_1^-, i.e., from the condition $\beta_- = 1$ (provided $x << f_0 - f$). The solution z_2^- exists only for observation points $z > f_0$, and therefore, regions 4 and 5 are separated by the straight line $x = (z - f_0)\tan\beta_0$, which follows from the condition $z_2^- = f_0$. In region 3, three solutions $z_1^{\pm}$ and z_2^+ exist simultaneously; this signifies the simultaneous crossing of three current tubes in a common ring. In this region, the highest current density

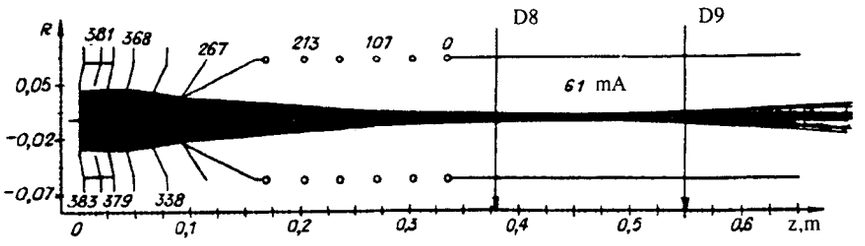

Fig. 1

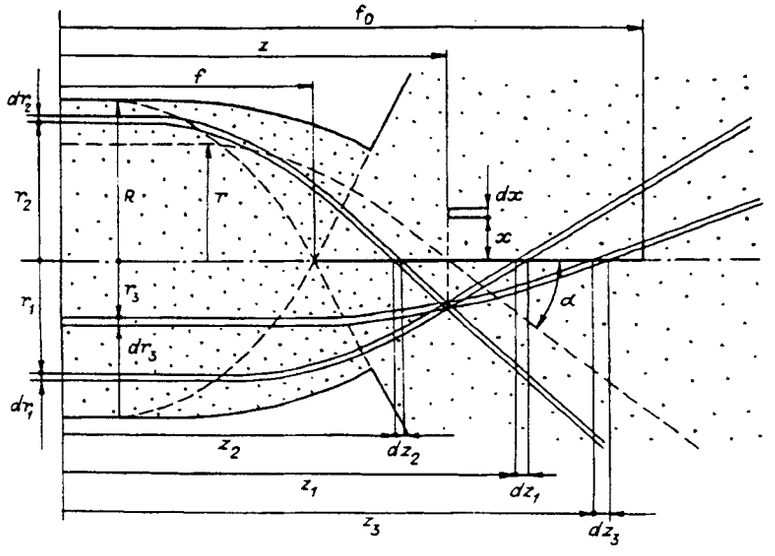

Fig. 2

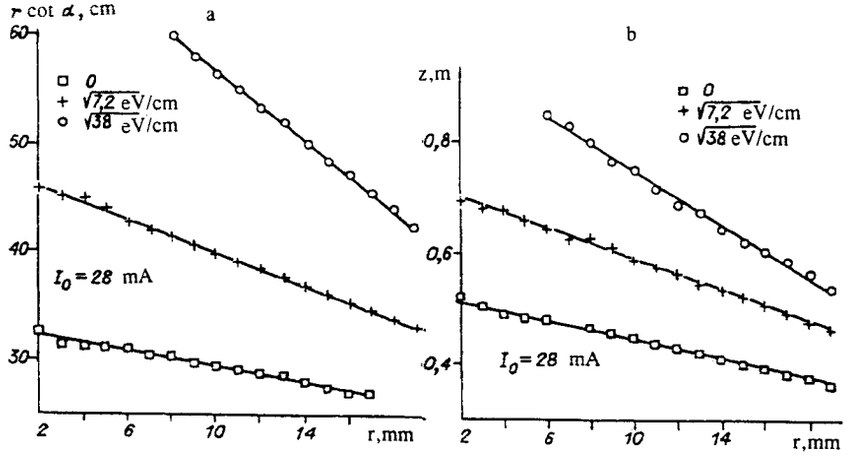

Fig. 3

and absolute crossover of the beam are observed. The crossover radius x_m and its position z_m on the axis can be determined from two conditions:

$$\beta_- = 1, \quad x = (z - f)\tan\alpha_0,$$

whence

$$x_m = (f_0 - f)\tan\alpha_0/(\sqrt{2} + \sqrt{1 + \tan\alpha_0 \cot\beta_0})^2,$$
$$z_m = f + x_m/\tan\alpha_0, \text{ where } \cot\beta_0 = -c > 0.$$

Table 1 gives the calculated parameters, characterizing the focusing of the proton beam, for three variants of the initial conditions, corresponding to Fig. 3a and b.

Figure 6a shows the profile of a 0.4-MeV proton beam with a current of 30 mA, obtained in the experiment of [1] with z = 645 mm and corresponding to the third calculated variant of Table 1. As is evident from Fig. 6, within the confines of the calculated crossover, there is about 90% of the total beam current, and the current density distribution is nearly hyperbolic. This is evident from a comparison of curves 1 and 2 in Fig. 6b, which correspond to the central portion of the beam, 5 mm in diameter, where curve 1 was obtained from the curve of Fig. 6a by subtracting the peripheral portion of the beam layer by layer, and curve 2 corresponds to the hyperbolic law of current density distribution in the beam. The presence of an extended, low-intensity peripheral portion in the experimental profile can apparently be explained by the influence of the particles from region 4.

Each value of $z_k^{\pm}$ is associated with a current density

$$j_k^{\pm} = j(r_k^{\pm}, 0)\frac{r_k^{\pm}}{x}\left|\frac{dr_k^{\pm}}{dz_k^{\pm}}\frac{dz_k^{\pm}}{dx}\right| = \frac{j(r_k^{\pm}, 0)}{2x}\frac{R^2}{(f_0 - f)^2}\frac{d(f_0 - z_k^{\pm})^2}{dx}. \tag{1.5}$$

Therefore, when the current density $j(r_k^{\pm}, 0)$ is equal to a constant value j_0, each value of $z_k^{\pm}$ will be associated with the following fraction of current in the aperture x:

$$\eta_k^{\pm} = [(f_0 - z_k^{\pm})/(f_0 - f)]^2. \tag{1.6}$$

The total current densities and current fractions in the aperture x in regions 1-5, according to Eqs. (1.5) and (1.6), will be, respectively:

$$\begin{aligned}
j_1 &= (j_0/2x)[(1/s_- - 1)bh + (s_- - 2 + 1/s_-)f_-ch^2],\\
j_2 &= (j_0/x)[(1/s_-)bh + (s_- + 1/s_-)f_-ch^2],\\
j_3 &= (j_0/2x)[(1 + 2/s_- + 1/s_+)bh + ((s_- + 1/s_-)f_-\\
&\qquad + (2 + s_+ + 1/s_+)f_+)ch^2],\\
j_4 &= (j_0/2x)[(1 + 1/s_+)bh + (s_+ + 2 + 1/s_+)f_+ch^2],\\
j_5 &= (j_0/2x)[(1 - 1/s_+)bh + (2 - s_+ - 1/s_+)f_+ch^2],\\
\eta_1 &= 0{,}25(1 - s_-)^2h^2, \quad \eta_2 = 1 - s_-h^2,\\
\eta_3 &= 0{,}25[(1 + s_+)^2g^2 - s_-h^2],\\
\eta_4 &= 0{,}25[(1 + s_+)g]^2, \quad \eta_5 = 0{,}25[(1 - s_-)u]^2,
\end{aligned} \tag{1.7}$$

where

$$h = R/(f_0 - f); \quad u = f_-/(f_0 - f); \quad g = f_+/(f_0 - f).$$

In Fig. 7a and b, the points represent the values of current fractions calculated from trajectories computed by the method of [6] for the injector of [2] at a proton current of 35 mA with a regular convergence of the beam particles at the injector input, 0.85 $eV^{1/2}$/cm, and which within the calculation error correspond to f = 31 cm, f_0 = 46 cm, R = 1.9 cm, b = 81 cm, c = −18. All these points lie on the corresponding curves of η vs x, obtained for different z in accordance with Eqs. (1.7), and this confirms their accuracy. Such an analytic calculation of current density is also useful, in particular, in

TABLE 1

Variant	$\sqrt{mv_z^2/2/r}$, $\sqrt{eV/cm}$	f	f_0	$f_0 - f$	$\cot \alpha_0$	$\cot \beta_0$	x_m	z_m
		cm					mm	
1	0	36,3	53,2	16,9	9,05	10,7	2,23	383
2	$\sqrt{7,2}$	45,3	72,8	27,5	16,25	7,5	2,46	493
3	$\sqrt{38}$	51,6	95,3	43,7	20,25	16,25	2,84	574

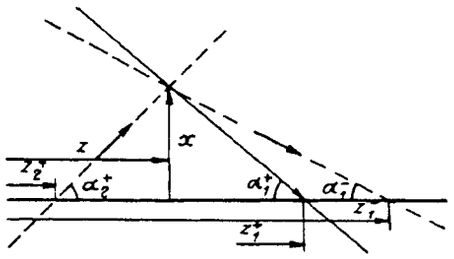

Fig. 4

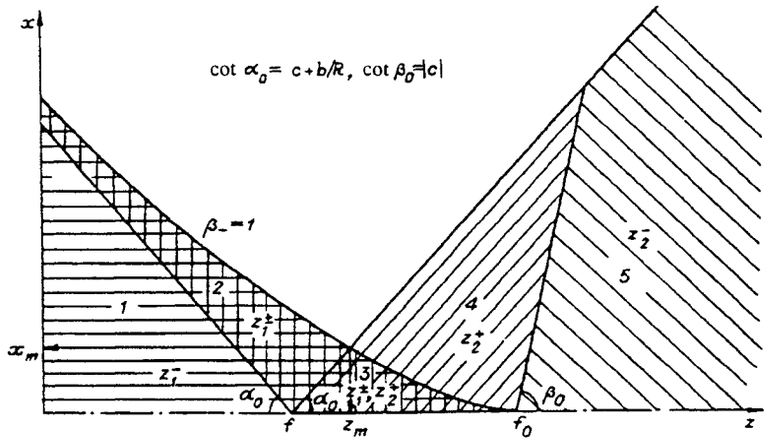

Fig. 5

that it makes it possible to determine the current through any area near the axis in the focusing region and near the surface $s_- = 0$, even though the current densities increase indefinitely as the axis in the focusing region and the surface $s_- = 0$ are approached.

2. Influence of Primary Beam Temperature on the Current Density Distribution in the Focused Beam. Particles of mass m having angular momentum M with respect to the axis travel past the latter at a minimum distance $a = M/mv_r$ ($v_r = v_z \tan \alpha$ being the radial velocity of the particles in the focusing region). Then

$$dI = j(x, z)2\pi x dx = \sum^{k} j(r_k, 0)2\pi r_k \left| \frac{dr_k}{dz_k} \frac{dz_k}{dy} \frac{dy}{dx} \right| dx, \tag{2.1}$$

where $y = \sqrt{x^2 - a^2}$ is the distance of the particle from the axis, its azimuthal motion being neglected (Fig. 8). It follows from (2.1) that

$$j(x > a, z) = \frac{1}{\sqrt{x^2 - a^2}} \sum^{k} j(r_k, 0) \left| \frac{dr_k}{dz_k} \frac{dz_k}{dx} \right|, \quad j(x < a, z) = 0. \tag{2.2}$$

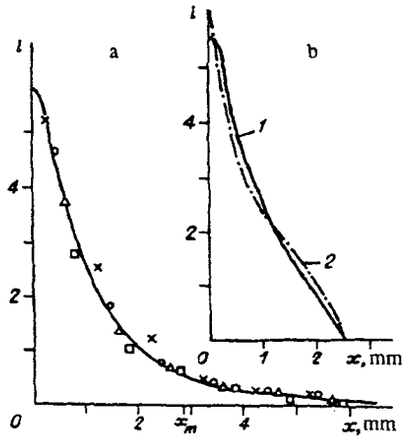

Fig. 6

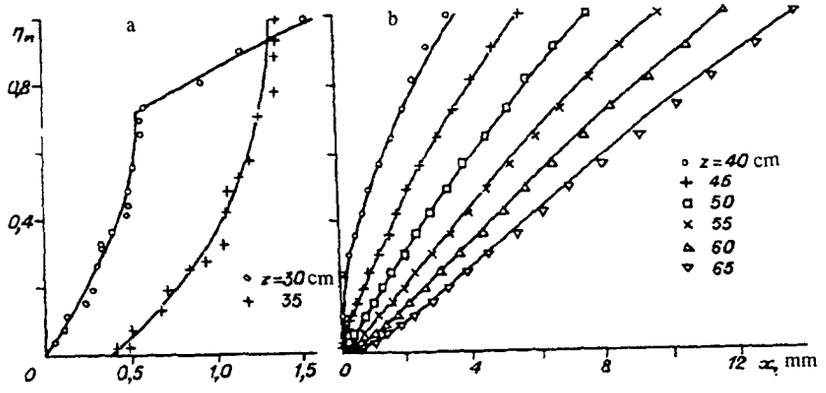

Fig. 7

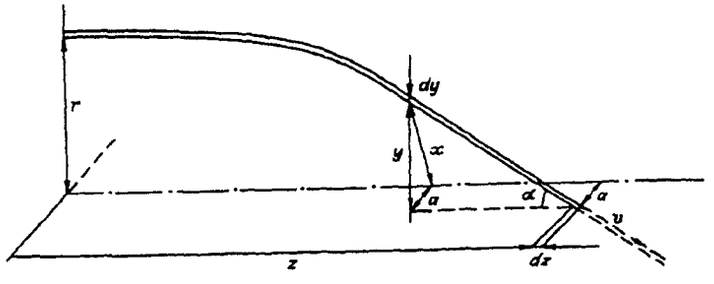

Fig. 8

Therefore, in the focusing region, as the axis is approached, the current density for x > a increases in accordance with the law

$$j(x, z) \to K(z)/\sqrt{x^2 - a^2}, \quad K = j(r, 0)\cot\alpha \left|\frac{dr^2}{dz}\right| \tag{2.2}$$

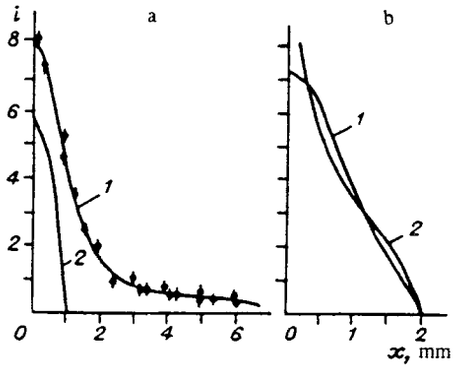

Fig. 9

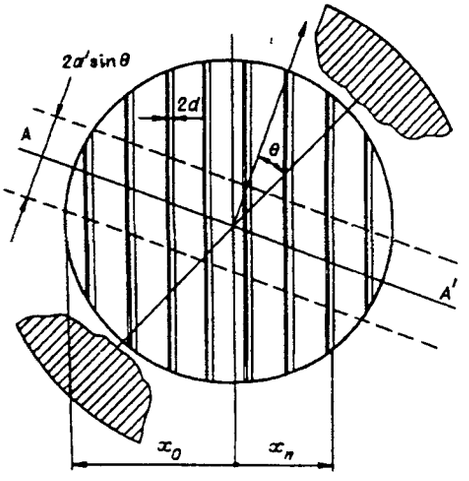

Fig. 10

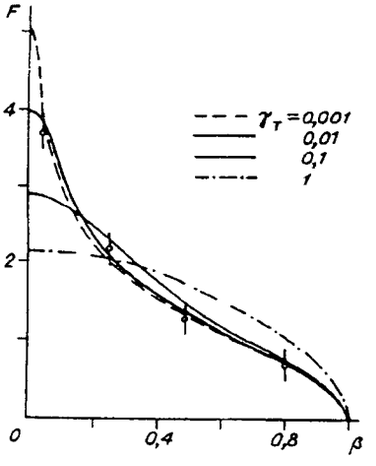

Fig. 11

and is zero when x < a. If the azimuthal velocities of the particles at the input have a distribution function $f(v_T)$, we obtain from (2.2)

$$j(x, z) \to K' \int_0^{v_r x/r} (x^2 - r^2 v_\tau^2 / v_r^2)^{-1/2} f(v_T) dv_\tau = (K' v_r / r) \int_0^1 \frac{f(v_r x\varepsilon / r) d\varepsilon}{\sqrt{1 - \varepsilon^2}},$$

and if the distribution function $f(v_T)$ has a Maxwellian form with temperature T, then

$$j(x, z) \to (\sqrt{2}\, K' / r \cot \alpha \sqrt{m\eta_T}) \int_0^1 \exp[-(\varepsilon x / r \cot \alpha \sqrt{\eta_T})^2] \frac{d\varepsilon}{\sqrt{1 - \varepsilon^2}}, \tag{2.3}$$

where $K' = K \sqrt{2m/\pi T}$; $\varepsilon = rv_T/xv_r$; $\eta_T = T/(mv^2/2) = T/\mathcal{E}$. Therefore, the maximum current density in the focusing region will be written [3]

$$j(0, z) = \sqrt{4\pi}\, j(r, 0) \left| \frac{dr}{dz} \right| \sqrt{\frac{\mathcal{E}}{T}},$$

and in the case (1.2)

$$j(0, z) = \sqrt{4\pi}\, j(r, 0) \frac{R}{f_0 - f} \sqrt{\frac{\mathcal{E}}{T}}. \tag{2.4}$$

Figure 9a shows a profile, obtained in the experiment of [3], of a 0.39-MeV proton beam with a total current of 75 mA, the central portion of which, bounded by a 2-mm radius (Fig. 9b), carries a current of 50 mA. The average current density in the region bounded by radius $r_0 = 1$ mm is $\langle j \rangle = 0.92$ A/cm^2, and the current density on the axis, which according to [3] reaches an almost constant level in the near-axis portion of the beam when $x < a_1 \approx 0.2$ mm, is

$$j_{av} = \langle j \rangle (r_0/2a_1)/(1 - a_1/2r_0) = 2{,}6 \text{ A/ cm}^2$$

The average current density on the emitter in this case is 6 mA/cm^2 and ranges from 7.5 mA/cm^2 on the beam axis to 3.75 mA/cm^2 on its periphery when R = 2 cm. The particle temperature on the emitter is T = 0.11 eV [3]. The beam-shaping regime corresponds to the regular radial divergence of the beam on the emitter $3\sqrt{\text{eV/cm}}$, and the shape of the trajectories, obtained in mathematical modelling, corresponds to the parameters $f_0 - f = 35$ cm. Then, according to (2.4), the current density on the axis of the focused beam should increase by a factor of $\sqrt{\pi\mathscr{E}/T} \cdot 2R/(f_0 - f) \approx 340$ and should change from 1.7 A/cm^2 when $z = f \approx 50$ cm to 3.3 A/cm^2 when $z = f_0 \approx 85$ cm. These calculated values of current density on the axis are in good agreement with the experimental value $j_{av} = 2.6$ A/cm^2 obtained when z = 64.5 cm, i.e., when $f < z < f_0$.

3. Influence of Primary Beam Temperature on the Focused Beam Profile. Wire sensors are used in the measurement of the beam profile [4, 5]. If the wires of the sensor are arranged in the aperture x_0 as shown in Fig. 10, then the current i_n from the n-th wire, separated from the center of the aperture by a distance x_n, the wire diameter being $d \ll x_0$, is related to the current density j(x, z) as follows

$$i_n = 2d \int_{x_n}^{x_0} j(x, z) x dx / \sqrt{x^2 - x_n^2}. \tag{3.1}$$

If the transverse temperature of the beam at the input is T, and the aperture x_0 is sufficiently small, is follows from Eqs. (2.3) and (3.1) that i_n and I_{x_0} (the current in the aperture x_0) are given by the formulas

$$i_n = (4Kd/\sqrt{\pi\gamma_T}) \int_0^1 \ln[(\sqrt{1 - \beta^2} + \sqrt{1 - \varepsilon^2})/\sqrt{|\beta^2 - \varepsilon^2|}\,] \exp(-\varepsilon^2/\gamma_T) d\varepsilon,$$

$$I_{x_0} = \int_0^{x_0} j(x, z) 2\pi x dx = (4Kx_0\sqrt{\pi}/\sqrt{\gamma_T}) \int_0^1 \exp(-\varepsilon^2/\gamma_T) d\varepsilon / \sqrt{1 - \varepsilon^2},$$

$$\gamma_T = (T/\mathscr{E})(r \cot\alpha / x_0)^2, \quad \beta = x/x_0.$$

Therefore, the fraction of the current flowing through the wire separated from the center of the aperture by a distance $x = \beta x_0$ is given by the formula

$$i/I_{x_0} = F(\beta, \gamma_T)(d/\pi x_0),$$

where

$$F(\beta, \gamma_T) = \frac{\int_0^1 \ln\left[(\sqrt{1 - \beta^2} + \sqrt{1 - \varepsilon^2})/\sqrt{|\beta^2 - \varepsilon^2|}\right] \exp(-\varepsilon^2/\gamma_T) d\varepsilon}{\int_0^1 \exp(-\varepsilon^2/\gamma_T) d\varepsilon / \sqrt{1 - \varepsilon^2}}.$$

Figure 11 shows the curves of F vs β for different γ_T, and the circles represent the F values obtained in the injector of [1] on the sensor located at a distance z = 645 mm from the inlet. The distance between the extreme wires of the sensor is $2x_0 = 8$ mm. The proton beam current is 28 mA, and the regular divergence of the beam at the entrance to the injector is 6 eV$^{1/2}$/cm. The proton source operated in a regime in which the proton scattering by the grid electrodes was substantially smaller than the thermal scattering [3]. As is evident from Fig. 11, within experimental error, the points fall on the $F(\beta)$ curve when $\gamma \leq 0.01$. This makes it possible to obtain the following upper limit of transverse temperature of the beam at the entrance to the injector:

$$T = \mathscr{E}\gamma_T (x_0/r \cot\alpha)^2 < \mathscr{E}\gamma_T [x_0/(b + cR)]^2 \leq 0{,}37 \text{ eV},$$

since the proton energy in the focusing region is $\varepsilon = 390$ keV, b $\approx$ 73 cm, c ≈ -16. The upper temperature limit obtained is in good agreement with the experimental results of [3, 4]. (*A* more accurate estimate is $T \approx \varepsilon_T[x_0/b + cr_m)]^2 \leq 0.24$ eV, where r_m corresponds to z_m.)

4. Influence of Particle Scattering near the Wire Electrodes Shaping the Beam on the Beam Profile in the Focusing Region. The wire electrodes forming the primary proton beam for further acceleration [3, 4] deflect the protons through a small angle $y\Delta E/2U$ (U is the accelerating voltage in the region of the grid fabric, ΔE is the difference between the electric field strengths before and after the wire cloth, and y is the distance from the passing protons to the nearest middle line between the wires). Therefore, the protons which have passed through the wire fabric have a uniform angular distribution in the range $\pm(s - d)\Delta E/4U$ (s being the spacing of the wires, and d, the diameter). In the beam-focusing region, this angular spread causes the axial symmetry of particle motion to break down. As a result, when the beam is shaped, the particles which previously moved strictly in the plane passing through the axis of the system begin to be scattered uniformly in the direction perpendicular to this plane, moving away from the latter according to the magnitude of the angular momentum, which they acquired as a result of scattering from the grid wires. According to the law of conservation of angular momentum of particles moving in central fields, we have

$$\sqrt{2eU/m}\,(s - d)(\Delta E/4U)\sin\theta \cdot mr = \sqrt{2eV/m}\,\sin\alpha \cdot am, \qquad V = \mathscr{E}/e. \tag{4.1}$$

Here r, θ are the polar coordinates of the particle on the emitter; a is the minimum distance of the particle from the axis of the system in the beam-focusing region. Considering that r >> s − d, we find that the particles located on the emitter in a plane AA′ characterized by angle θ (see Fig. 10) will, in the focusing region, be uniformly distributed in the vicinity of this plane of dimension $\pm a' \sin\theta$, where, according to (4.1),

$$a' = (s - d)(r/\sin\alpha)\Delta E/(4\sqrt{UV}).$$

The current density in the focusing region will be dependent on both the observation distance x from the axis and observation angle θ. A contribution to the current in the vicinity of the point x, θ will be made by particles which were located on the emitter in planes characterized by angles $\theta_- < \theta < \theta_+$, whence, because of the distance in the direction perpendicular to the plane, the particles can reach the point x, θ. Therefore, the values θ_+ and θ_- can be obtained from the conditions

$$a' \sin\theta_\pm = \pm x \sin(\theta_\pm - \theta). \tag{4.2}$$

The total current density in the vicinity of the point x, θ is given by an integral of the form

$$j(x, \theta) = \text{const}(a') \int_{\theta_-}^{\theta_+} d\theta/\sin\theta,$$

where the value const(a′) is obtained from the passage to the limit $j(x, \theta) \to K_1/x$ when $a' \to 0$, and the value of K_1 is specified by the condition

$$I_{x_0} = \int_0^{x_0} j(x) 2\pi x dx,$$

whence

$$j(x, \theta) = (I_{x_0}/4\pi x_0 a') \int_{\theta_-}^{\theta_+} d\varphi/\sin\varphi = (I_{x_0}/4\pi x_0 a')\ln(\text{tg}(\theta_+/2)\cot(\theta_-/2)). \tag{4.3}$$

It follows from (4.2) and (4.3) that

$$j(x, \theta) = (I_{x_0}/4\pi x_0 a')\ln\left(\frac{a'/x + \cos\theta + \sqrt{(a'/x)^2 + 2(a'/x)\cos\theta + 1}}{\sin\theta}\right).$$

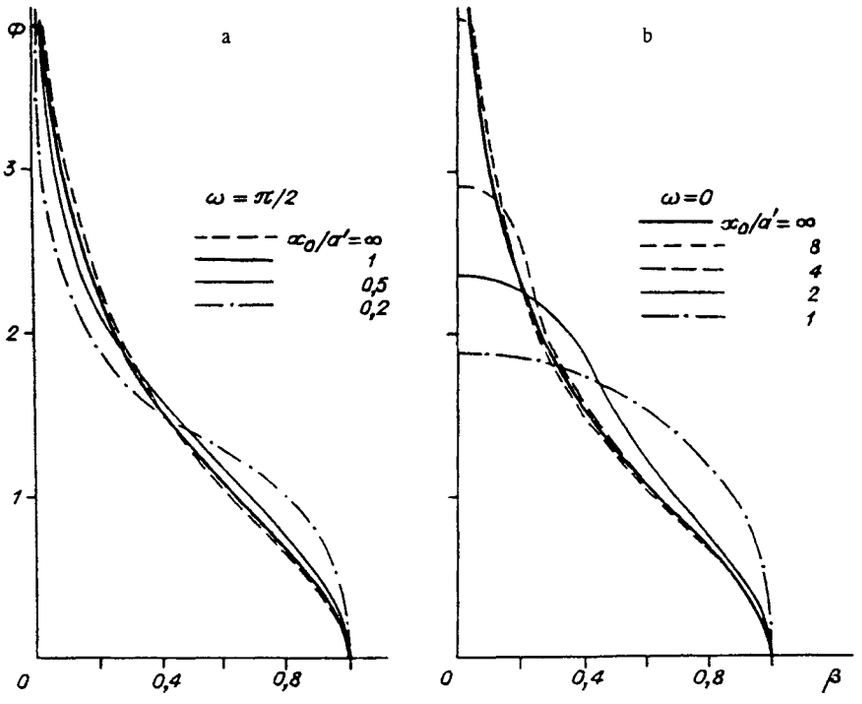

Fig. 12

Therefore, the fraction of the current flowing through the wire of the beam profile sensor, separated from the aperture center by a distance $x = \beta x_0$ and located at an angle ω to the filaments of the grid electrode forming the primary beam, is given by the formula

$$i_n / I_{x_0} = (d/\pi x_0)\Phi(\beta, x_0/a', \omega)$$

$$(\Phi = 0{,}25(x_0/a')\int_{-\varphi_0}^{\varphi_0} j(\cos\varphi/\beta(x_0/a'), \omega + \varphi)d\tan\varphi,\ \cos\varphi_0 = \beta).$$

Figure 12a and b gives the curves of Φ vs β for $\omega = 0$ and $\pi/2$, respectively, for characteristic values x_0/a' corresponding to high scattering ($x_0/a' \sim 1$) and low scattering ($x_0/a' >> 1$) by the grids. Figure 12a gives the projection of the beam profile along the filaments of the grid electrode, when the influence of scattering by the grids is minimal, and Fig. 12b shows the projection of the profile in the projection orthogonal to these filaments, when the scattering by the grids can considerably expand the beam profile, as is evident from the variants corresponding to the values $x_0/a' \gtrsim 1$.

In the injector used in [2], the distance between the grid electrodes is H = 1.4 cm. The grid diode shaping the primary proton beam operated at a current determined by the "three halves" rule, when the plasma boundary was located in the plane of the cathode grid, and the protons were scattered mainly by the filaments of the second grid electrode [3]. The spacing of the filaments was s = 0.225 mm, and the diameter was d = 0.05 mm. The voltage between the electrodes was U = 7.5 kV. The sensor aperture radius was x_0 = 8 mm. In that case, the inequality $r/\sin\alpha \leq \cot\alpha = b + cr < b$ being taken into account, the quantity x_0/a' satisfies the condition

$$x_0/a' > (16/3)[H/(s-d)](x_0/b)\sqrt{V/U} \approx 14.$$

As is evident from Fig. 12, when $x_0/a' > 14$, the two projections of the beam profile, taken when $\omega = 0$ and $\pi/2$, are very close to the curves with no scattering, when $x_0/a' = \infty$, and therefore practically coincide. Consequently, scattering by the grids is insignificant against the background of the thermal spread of the transverse particle velocities. The calculation makes it possible to refine the conditions necessary for shaping beams with a high degree of axial symmetry, obtained in experiments with a high-voltage proton accelerator [2].

REFERENCES

1. V. N. Getmanov and O. Ya. Savchenko, "Use of a grid-stabilized plasma emitter in a system for shaping a high-energy proton beam," Problems of Atomic Science and Technology, Nuclear Physics Research Series, No. 5/5 (1989), pp. 24-29.
2. V. I. Batkin, V. N. Getmanov, I. M. Ikryanov, and O. Ya. Savchenko, "Controlled-current pulsed proton accelerator," Prib. Tekh. Éksp., No. 2, 27-31 (1991).
3. V. N. Getmanov and O. Ya. Savchenko, "Distribution of current density in the beam of a high-voltage proton accelerator," Prib. Tekh. Éksp., No. 5, 34-40 (1992).
4. V. N. Getmanov, "Distribution of current density in the beam of an arc proton source," Zh. Prikl. Mekh. Tekh. Fiz., No. 1, 3-8 (1991).
5. V. N. Getmanov, "Small-sized sensor of current and profile of a pulsed proton accelerator beam," Prib. Tekh. Éksp., No. 1, 39-43 (1985).
6. V. Ya. Ivanov, Automation of Computer Design of Electronic Instruments, Preprint/USSR Academy of Sciences, Siberian Branch, Computing Center, No. 40, Novosibirsk (1977).